Numerical analysis of the thermoaeraulic behavior of air during the opening of the door of a refrigerated truck trailer equipped with cold plates

Jihyuk Jeong, Alla Eddine Benchikh Le Hocine, Sergio Croquer, Sébastien Poncet, Benoit Michel, Jocelyn Bonjour

Numerical Analysis of the Thermoaeraulic Behaviour of Air During the Opening of the Door of a Refrigerated Truck Trailer Equipped With Cold Plates

Jihyuk Jeong[a,b,*], Alla Eddine Benchikh Le Hocine[a], Sergio Croquer[a], Sébastien Poncet[a], Benoit Michel[b], Jocelyn Bonjour[b]

[a] *Mechanical Engineering Department, Université de Sherbrooke, 2500 boulevard de l'Université, Sherbrooke (QC) J1K 2R1, Canada*
[b] *Univ Lyon, INSA Lyon, CNRS, CETHIL, UMR5008, 69621 Villeurbanne , France*

Abstract

The present work reports the numerical simulation of the heat transfer inside a refrigerated truck trailer equipped with three eutectic plates and fans. The numerical model solves the conjugated heat transfer inside the trailer under unsteady conditions. The conservation equations of mass, momentum and energy are solved in 3D and closed using the $k-\omega$ Shear Stress Transport (SST) model. It is first favorably validated against the numerical and experimental data of Lafaye de Micheaux et *al*. [1]. The results are then extended to investigate the performance of a refrigeration system equipped with eutectic plates for the transport of frozen food products. As no significant 3D effects are reported, a 2D model is adapted to analyze the configurations with the plates placed in series on the roof of the trailer or vertically at its back. During the door opening period, the configuration with the plates placed on the roof without the cargo leads to noticeably lower area-averaged temperatures inside the trailer than the configuration with the plates placed on the back due to the presence of recirculation zones and the cold plates located near the doorway. However, the presence of the cargo eliminates the formation of these zones that limits the infiltration of the outside atmospheric air. Also the configuration with the plates placed in the roof allows the outside atmospheric air to infiltrate earlier, resulting in an overall higher temperature observed for the cargo.

Keywords: refrigerated truck trailer, eutectic plates, infiltration load, turbulence modeling

1. Introduction

Around 2 % of the total greenhouse gas emissions in developed countries are due to food transportation, including motive power and refrigeration [2]. Road transport refrigeration equipment needs to operate reliably in harsher environments compared to stationary one. For temperature-controlled transport vehicles, legislations exist and provide common standards and certifications [3]. ATP [3] (International Carriage of Perishable Foodstuff agreement) regulates the practice of transporting perishable foodstuffs in 48 countries. Despite the operating conditions required to preserve the cold chain, constraints due to available space, noise

*Corresponding author. Tel.:+1 514 817 2260. E-mail address: jihyuk.jeong@usherbrooke.ca.

and weight makes them less efficient than stationary systems. For road transport vehicles, different types of refrigeration units are employed mainly depending on the size of the vehicle and its load: vapour compression systems with a vehicle or an auxiliary alternator unit, a direct belt drive or an auxiliary diesel unit. For medium to large vehicles, refrigeration units powered by a self-contained diesel engine are primarily used. To guarantee $-20\,^{\circ}\mathrm{C}$ within the trailer, the fuel consumption is typically up to 4 liters per hour for a semi-truck trailer with an inside volume of $78.79\,\mathrm{m}^3$ [2].

Eutectic systems appeared as a valuable alternative to reduce or annihilate this fuel consumption. They typically consist of tubes, beams or plates filled with a Phase Change Material (PCM). During the typical delivery cycle, the eutectic plates absorb heat infiltrated into the trailer as latent heat and produce cooling to ensure the desired temperature inside the trailer. Such systems may be suitable for short distance deliveries. However, the heat losses through frequent door openings are a major concern, especially in humid climates. Frequent door openings account for the majority of the heat infiltration during delivery as well as inducing condensation and formation of frost along the plates. Thick condensed frost layers may block the heat transfer with the surrounding air and nullify its effects. It has never been studied experimentally, only preliminary numerical modelings have been published so far in similar configurations [4, 5].

Recently, application of PCMs for the walls of refrigerated vehicles have been proposed by various researchers [2, 6, 7, 8, 9]. Tinti et *al.* [7] investigated the characteristics of rigid polyurethane (PU) foams containing MicroPCM, respectively. They found that the thermo-regulating and thermal energy storage capacities of PU-PCM foams increases with increasing PCM content. Copertaro et *al.* [8] and Michel et *al.* [9] investigated the thermal performance of a sandwich structured PU-PCM insulation walls for refrigerated vehicles. The thermal performances of different PU-PCM configurations for varying PU/PCM layer thickness, PCM selection, ..., were analyzed for the entire day (24 hours). However, none of the aforementioned studies analyzed the heat transfer inside the refrigerated vehicle.

The heat and mass transfers inside a refrigerated chamber exhibit some similarities with those in a truck trailer and have received much more attention, especially for large refrigerated warehouses with short opening times. For a warehouse (about 13000 m^3, opening time lower than 1 min), Azzouz et *al.* [10] highlighted that the infiltration reaches a steady-state in less than 3 s, to be compared with 13 s for the temperature field. Many expressions of the steady-state heat infiltration rate based on the ideal flow theory have been then developed highlighting the influence of the door opening [11]. For smaller cold rooms or containers, Hoang et *al.* [12] studied numerically the 3D air flow in a refrigerated store either empty or with cargo using a RNG k-ε model. The authors regretted its poor performance and attributed it to the use of a coarse mesh (167152 elements in 3D). Foster et *al.* [13] investigated experimentally and numerically the heat and mass transfers between a refrigerated store (106 m^3, $-20°C$) and outside air at $20°C$ infiltrated through a 7.4 m^2 door (partially or totally opened). The fans were stopped 30 s before the door opening. The infiltration rate increased linearly with the opening time up to 18 s before reaching an asymptotical value corresponding approximately to 90% of the inside chamber volume.

On the contrary, there is a limited number of studies investigating the heat and mass transfer inside a truck trailer with frequent door openings. Tso et *al.* [14] experimentally investigated the influence of air, fan and plastic strip air curtains on the air infiltration through the 0.9 m^2 doorway of a 7.2 m^3 refrigerated truck body subject to typical conditions encountered in Singapore. The deployment of an air curtain can save up to 40% and 11% of energy compared to cases without an air curtain and a plastic strip curtain, respectively. They proposed also some numerical results which compare reasonably well with temperature measurements. Clavier et *al.* [15] experimentally investigated the infiltration through the doorway of a medium-size refrigerated truck placed in a wind tunnel. They compared the heat load with and without two types of air curtain. Their experiments showed that for the unprotected door and an opening time of 18 min, the average infiltration heat load is about 5.7 kW. More recently, Lafaye de Micheaux et *al.* [1] numerically and experimentally investigated the velocity and temperature distributions in a truck trailer with different door openings. Their experiments were performed on an insulated body with an inner volume of 32 m^3 with full, 2/3 lateral, 1/3 lateral and 1/3 central aperture door opening areas. The unsteady mass exchange driven by the density difference across the door, called buoyancy driven flow, extends to about 20 s for the full door opening and up to 50 s for 1/3 aperture ratio door opening. It is followed by the heat exchange between the outside air and the inner walls due to natural convection, which occurs as the temperature inside the container reaches a ceiling temperature of a few Kelvin below the outside air temperature. Finally, a quasi-steady state heat transfer was observed until the doors are closed. Lejeune [16] performed a complete experimental and theoretical analysis for three systems, named fully eutectic, semi-eutectic and roll-bond. His nodal model has been applied to a complete delivery cycle. The results being confidential cannot be used here for comparison purpose. Rai et *al.* [17, 18] investigated numerically the performance of an air curtain for a 44.2 m^3 refrigerated truck trailer using a 3D standard k-ε model and first-order discretization schemes. They considered door openings during up to 15 min and two trailer configurations without and with cargo. Natural infiltration is found to be mainly caused by the cold air flow going out from the lower part of the door. An air curtain at an optimum averaged velocity of 3.1 m/s placed inside the trailer reduced the energy consumption by 48% [17]. They also considered two different positionings of the air curtain, inside or just outside the trailer. When placed outside, the air curtain outperformed the base case with the curtain placed inside by 8% in terms of energy performance [18]. Ben Taher et *al.* [19] numerically determined that for a closed-door refrigerated truck, there was no significant difference between the different turbulence models (standard k-ω, k-ω SST, and stand k-ε) and the measured temperature against the experimental results of Jara et *al.* [20]. However, the root-mean-square-error values obtained with the k-ω SST model showed a better agreement. Croquer et *al.* [4] proposed preliminary CFD results for a truck trailer equipped with eutectic plates placed at the back of the trailer. Their k-ω SST turbulence model with an appropriated mesh distribution slightly improved the predictions of the realizable k-ε model of Lafaye de Micheaux et *al.* [1]. Then, they optimized the interplate distance and the geometry of the separating wall. An interplate distance of 0.06 m resulted in the lowest average temperature in the loading region compared to the cases with an

interplate distance of 0.036 m and 0.10 m. It has been later extended by Bonaventure et *al.* [5] for the case with the plates placed at the roof of the trailer and for a configuration with cargo.

The main objective of this study is to analyze the flow field, temperature distribution and infiltration heat load into the system during the door opening period for a truck trailer refrigerated with three eutectic plates and loadings. Lafaye de Micheaux et *al.* [1] performed so far the most complete analysis on a similar configuration. Compared to these authors, the main originalities come from the addition of three eutectic plates and fans, the comparison between two configurations for the plates (located at the back or at the top of the trailer), and two modes for the fans (blowing and suction) and the presence of loadings. To the best of the authors knowledge, such a detailed analysis has never been performed so far.

2. Numerical modeling

In the following section, the geometrical configuration is first described in detail. The numerical methodology (algorithms, numerical schemes) as well as the numerical parameters, including the mesh grid and the boundary conditions are then presented.

2.1. Geometrical modeling

The computational domain is a truck trailer of length 7.13 m and height 2.62 m. The refrigeration system includes three eutectic plates of thickness 0.054 m and height/length 1.76 m and fans, which maintain the air circulation through the plates and the container when the doors are closed. Figure 1a displays the two configurations assessed here: plates placed vertically in parallel at the back of the trailer (Configuration A) and plates in series located at the roof (Configuration B). For each configuration, two air circulation modes are employed, namely the blowing and suction modes. For the blowing mode, air is blown out from the plate region to the trailer and for the suction mode, air is sucked into the plate region. The truck trailer is placed in a wind tunnel of length 31 m and height 5.43 m maintained at 293 K with a zero velocity field (Fig.1b).

The plates are maintained at 244 K, which corresponds to the melting point of a typical sodium-chloride mixture as a phase change material (PCM). The plates have been designed such that the system can operate during a whole working day of 8 hours. Mousazade et *al.* [21] employed a plate partially filled with 35 kg of PCM E-29 (from the available space for 81.01 kg) with the length of 1.59 m and the thickness of 0.052 m and observed full melting of the PCM after apprxoimately 3.33 hours for a closed truck configuration with the volume of 21.65 m^3. By employing three plates filled with a PCM with similar dimensions as Mousazade et *al.* [21], PCM is assumed to not have fully melted during the 8 hours of operation. The assumption of a constant temperature for the plates is assumed to be valid as it is a mixture of solid and liquid in thermal equilibrium. The wall that separates the eutectic plates from the loading area of the trailer is 1.81 m in length and 0.01 m in thickness for Configuration A and 5.45 m in length and 0.01 m in thickness for Configuration B. For both configurations, a distance of 0.06 m is maintained between the wall and the plates based on the former results of Croquer et *al.* [4].

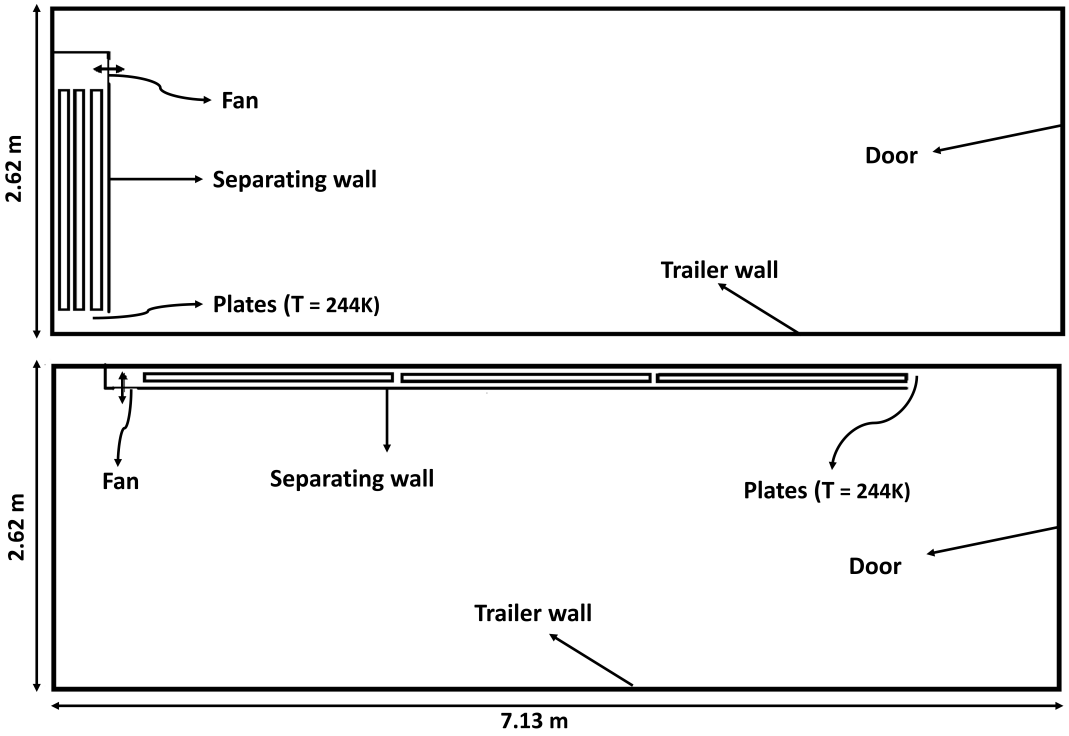

(a)

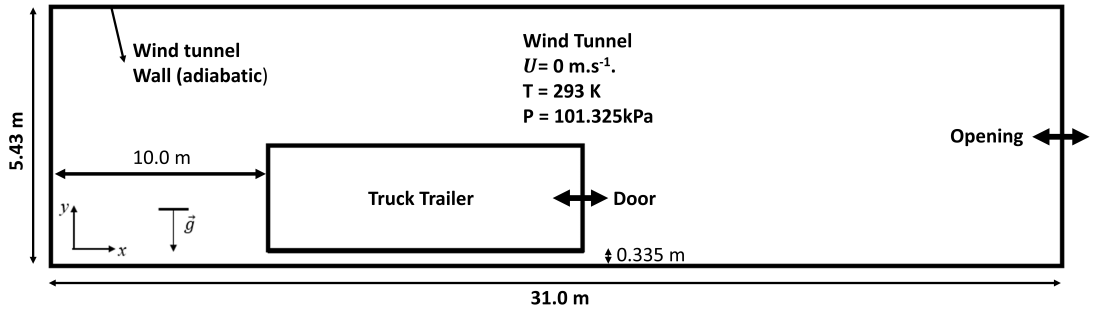

(b)

Figure 1: (a) Trailer diagram with the position of the eutectic plates for Configuration A (top) and Configuration B (bottom) (b) General schematics of the computational domain with the relevant boundary conditions.

Figure 2 shows the details of the optimized plate system design obtained by Croquer et *al.* [4]. The dimensions, which are based on commercially available plates and truck container models, are summarized in Table 1. The inter plate spacing is set to 0.06 m as for the distance between the plates and the walls.

2.2. Numerical method

The conservation equations for mass, momentum and energy are solved using the finite-volume method. Second-order upwind and centered schemes are preferred respectively for the spatial discretization of the

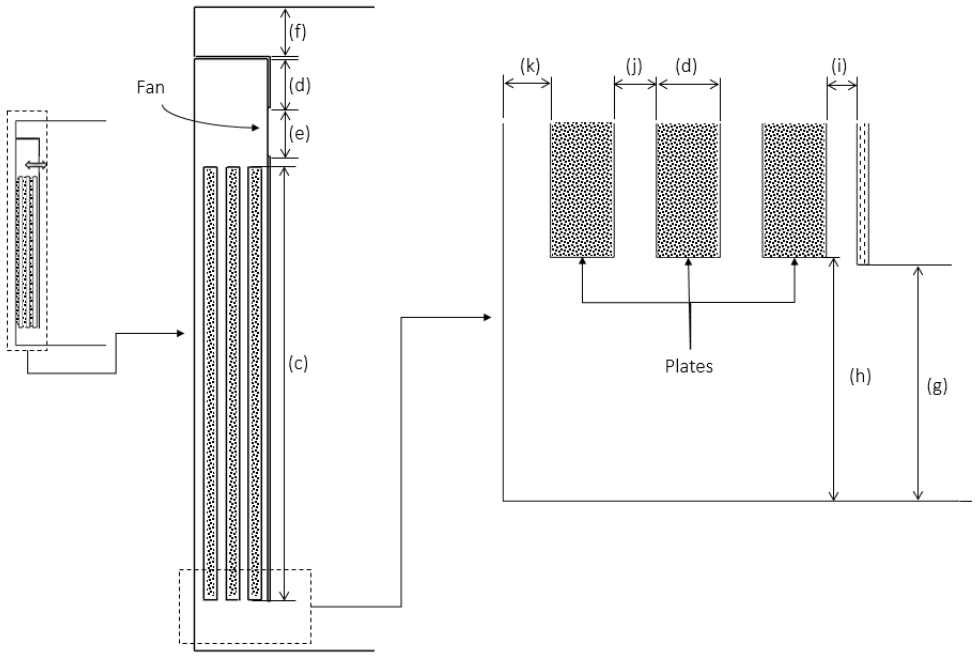

Figure 2: Details and dimensions of the eutectic plates.

Feature	**Distance** [m]
Container length (a)	7.13
Container height (b)	2.62
Plate thickness (c)	0.054
Plate height (d)	1.76
(e), (f), (g), (h)	0.2, 0.345, 0.2, 0.206
(i), (j), (k)	0.06, 0.06, 0.06

Table 1: Container and eutectic plate dimensions.

advection and diffusion terms, while a second-order Backward-Euler scheme with implicit time-stepping is used for the temporal discretization. The pressure-velocity coupling is overcome using a Rhie-Chow fourth-order algorithm.

The flow field is modeled by solving the (un)steady-state Reynolds Averaged Navier-Stokes equations (URANS) including the thermal energy equation, as the kinetic energy effects are negligible. Buoyancy air-driven flows with a maximum temperature difference of 29 K are expected, therefore air may be assumed to behave as an ideal gas with variable density and constant transport properties and the Boussinesq model accounts for the density change [22]. Turbulence effects are modeled using the Shear Stress Transport k-ω model developed by Menter [23] with production terms representing buoyancy contributions to the turbulent field. The k-ω SST model applies the robust k-ϵ formulation in the free turbulence regions and the more near-wall accurate k-ω model within the boundary layers, depending on a wall-distance weighted function.

All calculations are performed using the commercial software *CFX ANSYS.v19*.

Influence of the solar irradiation and the speed of the truck trailers has not been included in this study. Glouannec et *al*. [24] numerically and experimentally determined that while the heat fluxes through the walls are significantly increased by the solar irradiation, it has small to negligible effect on the temperature of the inner insulating wall of the refrigerated truck. Therefore, influence of the solar irradiation on the temperature distribution inside the refrigerated truck were deemed negligible. Mousazade et *al*. [21] experimentally determined that the overall heat transfer coefficient of the system increases as the speed of the truck increases. However, increase in the speed of the truck from approximately $80\,\mathrm{km\,h^{-1}}$ to $112\,\mathrm{km\,h^{-1}}$ only resulted in the increase of the overall heat transfer coefficients by $0.015\,\mathrm{W\,m^{-2}K^{-1}}$, $0.028\,\mathrm{W\,m^{-2}K^{-1}}$, and $0.023\,\mathrm{W\,m^{-2}K^{-1}}$ for the three PCM systems tested. Furthermore, as the current study is validated and compared against the published works that does not include solar irradiation nor the speed of the truck, there were excluded for validation and comparison purposes [1, 13, 17, 18].

2.3. Numerical parameters

Unstructured meshes of triangular (resp. tetrahedral) elements are generated for the spatial discretization of the 2D (resp. 3D) domain, with a minimum of 10 prismatic layers close to all solid boundaries with a growth rate set to 1.1 as well as local refinement in the door interface region. To perform 2D simulations on *CFX ANSYS.v19*, the 2D mesh was extruded in the normal direction by two elements for a total thickness of 0.02 m. Translational periodic boundary conditions are imposed on both faces of the extrusion. A mesh-sensitivity analysis was carried out in the 2D configuration to determine the minimum element size. A mesh grid composed of about $\sim 9.0 \times 10^5$ elements has proven to provide grid-independent results while guaranteeing a maximum dimensionless wall coordinate y^+ to be always lower than 1, a prerequisite for the use of a low-Reynolds number approach. Details of these mesh grids are displayed in Figure 3.

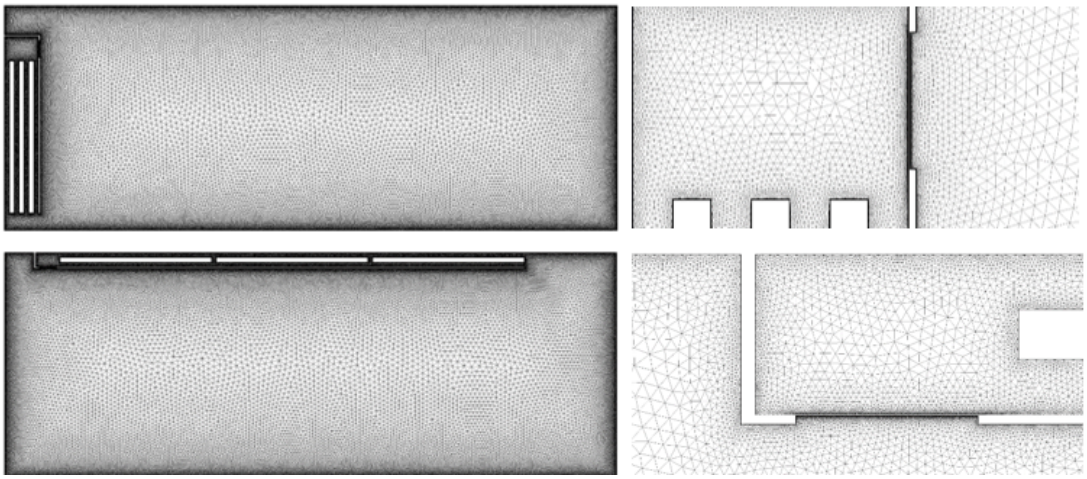

Figure 3: Overview of the mesh grids for Configuration A (top) and Configuration B (bottom) with a focus on the fan and the plate regions on the right.

Steady-state calculations are performed on a 2D domain as shown in Figure 3. An overall external heat transfer coefficient $h = 0.4\,\mathrm{W\,m^{-2}K^{-1}}$ corresponding to a heavily insulated equipment is imposed on the external walls [5], with an outside atmospheric temperature of 293 K to model thermal resistance of the walls and the air outside trailer computational domain. The separating wall is made of polypropylene with a thermal conductivity of $1.4 \times 10^{-4}\,\mathrm{W\,m^{-1}K^{-1}}$ and a specific heat of $1800\,\mathrm{J\,kg^{-1}K^{-1}}$. Regarding the ventilation system, the need for accurately modeling the fans is avoided by inserting a source term in the momentum equation over a surface representing the fan diameter of 0.2 m , such that the air passing through the fans is accelerated to an averaged horizontal velocity of $8.4\,\mathrm{m\,s^{-1}}$ in a prescribed direction. Hoang et *al.* [12] modeled also the fans through a source term in the momentum equation but based on a quadratic law giving the pressure losses overcome by the fan as a function of the superficial velocity. The steady-state calculations are initialized with a constant pressure of 101.325 kPa, an initial trailer temperature of 253 K and a zero-velocity field ($\vec{V}_{init} = \vec{0}\ \mathrm{m\,s^{-1}}$).

For the transient simulations during the door opening period, the truck trailer is placed inside the wind tunnel displayed in Figure 1. All wind tunnel walls are assumed to be adiabatic with an opening boundary condition in CFX imposed on the rightmost surface, with $T_{opening} = 293$ K and $P_{opening} = 101.325\ kPa$. The direction of the flow is specified to be normal to the boundary condition and the magnitude of the velocity is solved as a part of the solution. The trailer is located 10.0 m away from the leftmost wind tunnel wall and 0.335 m above the floor of the wind tunnel. A wall equivalent thermal resistance of $1.84\,\mathrm{m^2\,K\,W^{-1}}$ is used to model the heat flux through the trailer walls. The initial conditions of the wind tunnel are fixed to be 101.325 kPa, 293 K and $0\,\mathrm{ms^{-1}}$ at $t = 0$ s. For the transient simulations, results from the steady-state simulations with the corresponding operating mode and configuration are used to initialize the flow field inside the trailer. Instantaneous door opening is assumed at $t = 0$ s and the fans are turned off. An adaptive time-step approach is adopted with 3 to 5 target inner-loop iterations and initial and maximum time steps equal to of 10^{-7} and 10^{-2} s, respectively. The convergence criteria for mass, momentum and energy residuals are fixed under 10^{-4}. This results in a typical time step of about 5×10^{-3} s. Simulations are performed using the HPC facilities of Calcul Québec using 20 to 40 CPU nodes with 12 *AMD Opteron 6172* cores 32 GB RAM per node.

3. Validation of the numerical model

In order to determine the optimal numerical setup offering good accuracy at the lowest computational cost, a preliminary benchmark is carried out involving two aspects: (i) 3D domain vs. 2D domain and (ii) heat conducting vs. adiabatic container walls. The present numerical model is validated against the experimental and numerical data of Lafaye de Micheaux et *al.* [1], which provided temperature and velocity profiles of the air flow inside an empty truck trailer without the eutectic plates. The configuration is shown in Figure 1. Its inner dimensions are $H = 2.35 \times W = 2.5 \times L = 5.51$ m. It is placed midway in a tunnel of $H = 5.43 \times W = 5.5 \times L = 31$ m at a distance of 0.35 m from the floor. In the baseline experiment, the

container and wind tunnel initial temperatures were respectively 253 K and 293 K. At $t = 0$ s, the container door was fully opened, and velocity and temperature measurements inside the container and at the door were logged for about 60 s and compared to the results obtained by the model of Lafaye de Micheaux et *al.* [1].

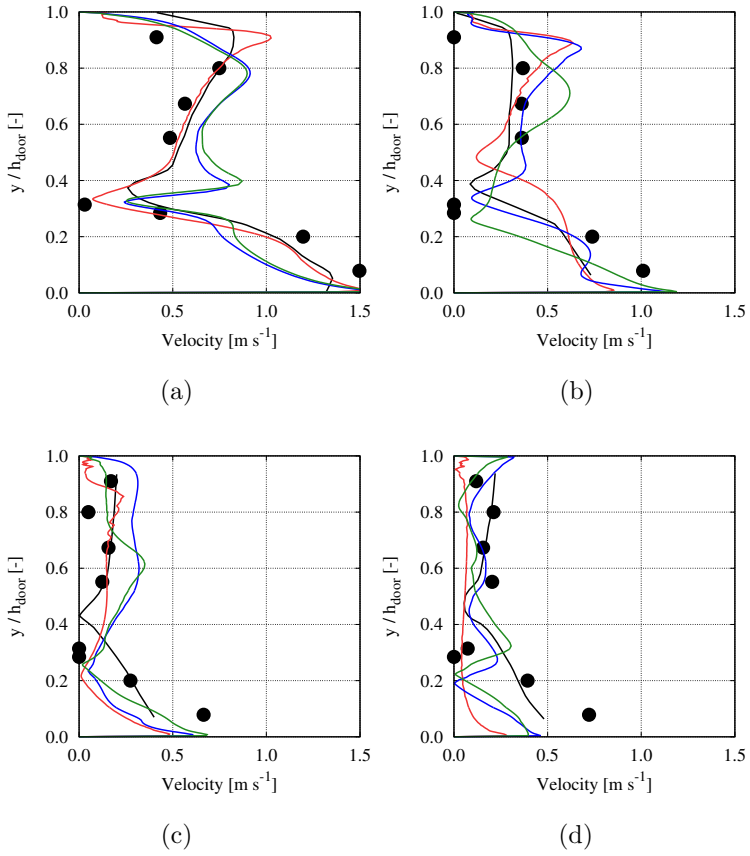

Figure 4: Comparison of the velocity magnitude profiles at the container door vertical centerline between the present simulations and the published data of Lafaye de Micheaux et *al.* [1] at (a) $t = 10$ s, (b) 20 s, (c) 40 s and (d) 60 s. Legend: • Experiment - Lafaye de Micheaux et *al.* [1], — CFD - Lafaye de Micheaux et *al.* [1], — CFD 3D, — CFD 2D with no heat transfer, — CFD 2D with heat transfer.

Unstructured meshes of triangular (resp. tetrahedral) elements are generated as described in Section 2.3. It results in mesh grids composed $\sim 1.46 \times 10^5$ and $\sim 1.34 \times 10^7$ elements for the 2D and 3D configurations, respectively. The boundary conditions are similar to the case with the eutectic plates (Fig.1b). The container walls are assumed to be either adiabatic or allowing for heat conduction with a wall equivalent thermal resistance of $1.84\,\mathrm{m^2\,K\,W^{-1}}$, value based on typical refrigerated container insulation layers [4]. Thus, one could compare the results against the regulatory requirements [3]. A general-connection interface is set at the container door to connect the meshes across the doorway and allow for the air to enter and exit through the interface and a symmetry condition is imposed at the mid-plane of the 3D case to reduce the computational cost.

For the benchmark study, three numerical configurations are considered: (i) 3D domain without heat

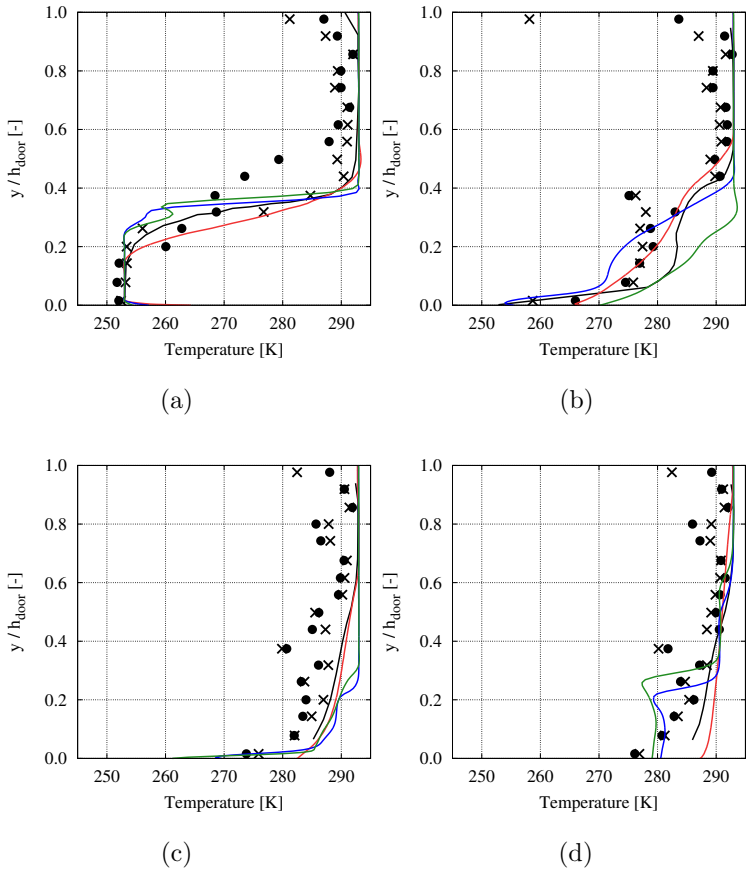

Figure 5: Comparison of the temperature profiles at the container door vertical centerline between the present simulations and the published data of Lafaye de Micheaux et *al.* [1] at (a) $t = 10\,\mathrm{s}$, (b) $20\,\mathrm{s}$, (c) $40\,\mathrm{s}$ and (d) $60\,\mathrm{s}$. Legend: • Experiment 1 - Lafaye de Micheaux et *al.* [1], × Experiment 2 - Lafaye de Micheaux et *al.* [1], — CFD - Lafaye de Micheaux et *al.* [1], — CFD 3D, — CFD 2D with no heat transfer, — CFD 2D with heat transfer.

transfer, (ii) 2D domain with heat conduction through the container walls and (iii) 2D domain with adiabatic walls. A comparison of the door velocity profiles at $t = 10$ s, 20 s, 40 s and 60 s after the door opening is shown in Figure 4. A good general agreement is observed in terms of both the instantaneous shape profiles and their temporal evolution. The 3D numerical setup seems to better fit the experimental data, in particular at $t = 10$ s and $t = 40$ s, nonetheless both 2D approaches show good accuracy and even a better capture of the velocity profile at $t = 60$ s.

Figure 5 compares the door temperature profiles for the same conditions described above. At $t = 10$ s, the air flow is yet in an early stage not far from the initial step profile, therefore no conclusive differences are seen. Nonetheless as the time passes, the profiles evolve into a curved shape with a maximum temperature of about 289 K, which all numerical approaches seem to over predict by about 1 K. At $t = 20$ s and $t = 40$ s, both 2D setups fail to fully replicate the experimental profile at the lower section ($y/h_{door} \sim 0.2$), this is particularly noticeable in the adiabatic walls setup at $t = 20$ s. Nonetheless the differences are of the same range as the dispersion of the experimental data. Deviations are also observed in the near-wall regions, particularly

for $y/h_{door} \rightarrow 1$, where the numerical models predict a constant wall temperature of 293 K whereas the experimental data reveal an important temperature gradient. The temperature gradient at the bottom is well captured, specially by the 2D models.

The numerical results showed a recirculation located at the door region which leads to turbulent fluctuations. The instantaneous profiles of Figures 4 and 5 show differences between the numerical and experimental results. This scattering might be attributed to the natural turbulent fluctuations, thus implying that the three numerical models are quite capable of capturing the main flow features across the door.

Further validation is shown in Figure 6 in terms of the infiltration rate. It is defined as the volume flow rate into the trailer across the doorway as follows:

$$\dot{V} = \iint v_n \, \mathrm{d}A_{door,infiltration} \tag{1}$$

with v_n the velocity normal to the doorway with the positive direction towards the trailer.

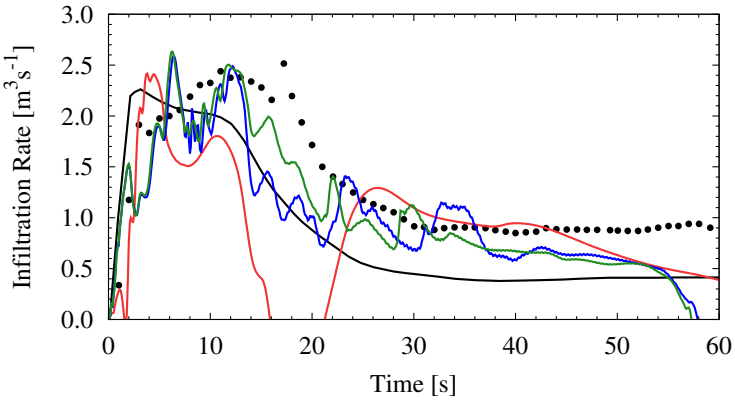

Figure 6: Comparison in terms of the infiltration rate at the container door between the present simulations and the experimental and numerical data of Lafaye de Micheaux et *al.* [1]. Legend: • Experiment 1 - Lafaye de Micheaux et *al.* [1], — CFD - Lafaye de Micheaux et *al.* [1], — CFD 3D, — CFD 2D with no heat transfer, — CFD 2D with heat transfer.

In Figure 6, the three numerical setups are able to properly capture the main features of the experimental results, in particular the initial flow acceleration and the time needed for reaching the steady state. The greatest difference is attained by the 3D model in the $t = 11$ s to 22 s period, which coincides with the passing of a large eddy across the door, implying recirculation and thus negative infiltration values for the given period. It is unclear if the experimental procedure properly reports these structures as the reported values are averaged over the door centerline, whereas the 3D results comprise a full integration over the door surface. This would also explain the better fit of the 2D models, which essentially represent the flow across the door vertical centerline.

In conclusion, although the 3D approach shows in general a better agreement with the experimental data, both in terms of velocity and temperature profiles across the door, it does not bring a significant improvement over the results obtained with the 2D models. Inclusion of the heat conduction across the container walls

introduces additional complications to the model. However, it has non-negligible effects during the delivery cycle and is specified by regulatory bodies [3]. Therefore, the 2D model with the heat conduction across the container walls was chosen to model the refrigerated container with the eutectic plates.

4. Results and discussion

Results are analyzed in this section for the truck container with the eutectic plates as described in Section 2. Steady-state calculations are initially performed for the two configurations with the plates located at the back (Configuration A) and the roof of the trailer (Configuration B) with two operating modes (Blowing and Suction). The aforementioned configurations are compared without and with a given cargo load. Afterwards, results obtained from the steady-state simulations are imposed as the initial values inside the trailer before the door opening for the transient calculations to investigate the interaction between the developed fluid flow inside the trailer and the infiltrating atmospheric air.

4.1. Configurations without cargo

Configurations A and B - suction and blowing modes are first compared for an empty trailer.

4.1.1. Closed trailer without cargo

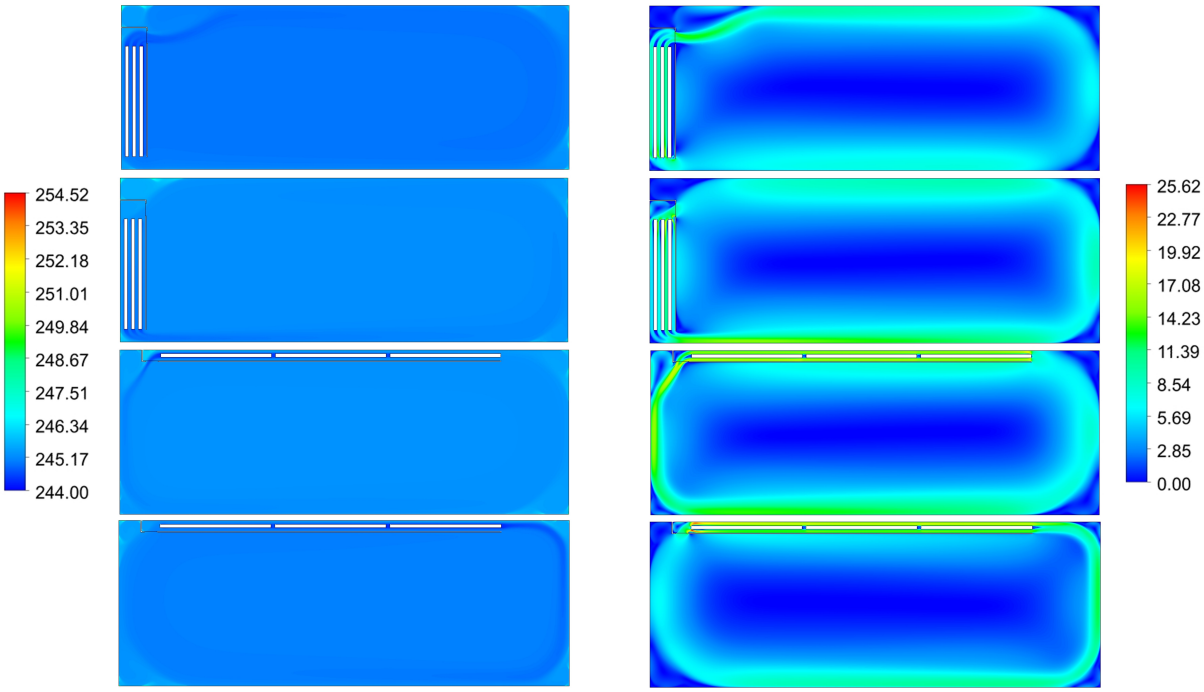

Figure 7: (a) Temperature [K] and (b) velocity magnitude [ms^{-1}] contours for Configurations A and B. The blowing mode is always on the top and the suction mode at the bottom.

Configuration	Maximum temperature [K]	Area-averaged temperature [K]	Area-averaged velocity [$\mathrm{m\,s^{-1}}$]
A - blowing	254.5	245.1	3.64
A - suction	252.1	245.6	4.21
B - blowing	253.5	245.4	4.30
B - suction	254.0	245.2	3.33

Table 2: Temperature and velocity magnitude obtained from the steady-state simulations.

From the results obtained from the steady-state simulations of Configurations A and B without the cargo, it appears that the temperature distribution inside the trailer is homogeneous with a near-zero velocity zone near the center of the trailer. This is observed in Figure 7 for both configurations and fan directions. Slight inhomogeneity of the temperature distribution is observed due to the recirculation zones at each corner of the trailer with the maximum temperature inside the trailer. Table 2 reveals that the difference in the plate location and the operating mode has negligible impact on the temperature inside the trailer for the steady-state simulations, as the maximum difference is 0.5 K for the area-averaged temperature over the cargo loading area (excluding the area occupied by the eutectic plates). The counterclockwise flow inside the trailer (Configuration A - suction and Configuration B - blowing) results in an overall lower area-averaged temperature and in a higher velocity inside the trailer. For all configurations and operating modes, the maximum temperatures inside the trailer are below the regulated cargo temperature of frozen foodstuffs at 261.15 K and quick (deep) frozen foodstuffs at 255.15 K [3]. Also, the homogeneity of the temperature field inside the cargo loading area respects the regulated maximum temperature difference of 2 K [3].

Also, there are few distinctions that can be observed between each configuration:

1. For Configuration A - blowing mode (Fig. 7), there is no flow between the rightmost plate and the separating wall, effectively reducing the influence of the plate. For Configuration B, all the plates are fully utilized.
2. For Configuration B - blowing mode, the flow velocity from the plates to the trailer is reinforced by gravity. On the contrary for the suction mode, the flow being dragged from the bottom of the trailer to the plates is weakened by gravity. Therefore, the highest area-averaged velocity is obtained for Configuration B - blowing mode and the lowest is obtained for Configuration B - suction mode. For Configuration A, gravity similarly reinforces and weakens the strength of the flow for the suction and blowing modes, respectively. However, the influence is weaker as the fans are located closer to the floor of the trailer.

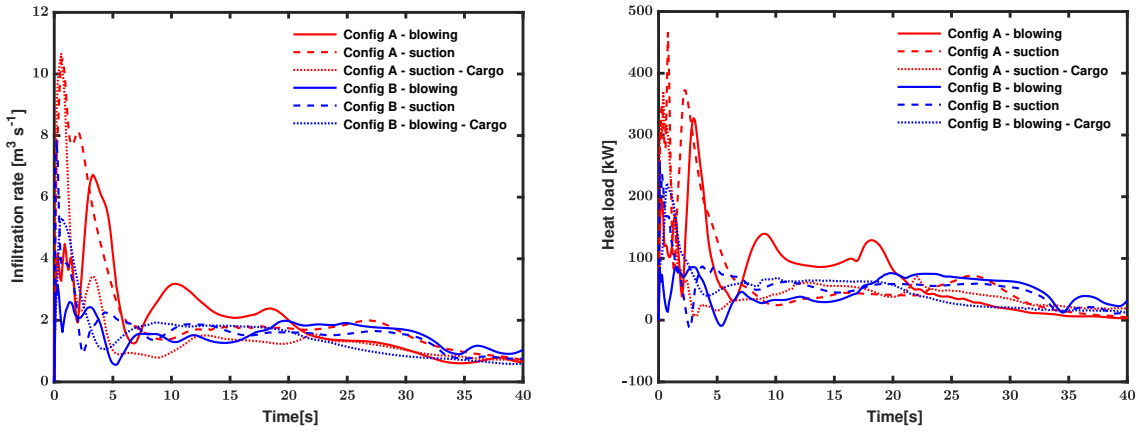

(a) (b)

Figure 8: Temporal evolutions of the (a) infiltration rate and (b) heat load through the door for the two configurations and modes.

4.1.2. Door opening period without cargo

The infiltration rate ($\dot{V}$) is defined as the volume flow rate of the air infiltrating into the trailer and the heat load ($\dot{Q}$) is defined as the amount of heat exchange occurring through the entire doorway. The calculation of the infiltration rate is defined in Eq. 1. The heat load across the doorway is calculated as:

$$\dot{Q} = \iint v_n \frac{P}{RT} c_{p,da} (T - 273)\, \mathrm{d}A_{door} \tag{2}$$

v_n is the velocity normal to the doorway with the positive direction towards the trailer, P the pressure, R = 287.085 J kg^{-1} K^{-1} the specific gas constant of dry air and $c_{p,da}$ = 1006 J kg^{-1} K^{-1} its specific heat. In Eq. 2, the reference temperature is chosen as 273 K. Note that the infiltration rate is defined as the volume flow rate into the trailer. However, for the heat load induced through the door, both exfiltration and infiltration through the door are accounted. To obtain the infiltration rate and the heat load across the entire doorway, the 2D values were scaled to that of 2.5 m in width as in Lafaye de Micheaux et *al.* [1] and Croquer et *al.* [4].

The renewal time is defined as the time required by the internal air to be completely renewed by the air from the outside the trailer[1]. As the simulations are initialized by the pre-existing flow from the steady-state results before the door opening, infiltration does not directly correspond to the amount of pure atmospheric air entering into the trailer. Especially in the first few seconds (t = 0 to $\approx$ 5.0 s) mixing of cold high-velocity air and the hot atmospheric air is prominent near the doorway and can be the main source of infiltration. For Configuration B (Fig.8b) with the blowing and suction modes at t = 5.3 s and t = 2.6 s respectively, the heat load induced through the door is negative as the exfiltration of high-temperature air occurs due to this interaction. However, it appears that for the majority of the simulation, the heat load induced through the door directly corresponds to the infiltration rate. Therefore, the infiltration rate and the renewal times from Figure 8a and Table 3 are used as the parameters to determine the performance of the configurations and

the operating modes.

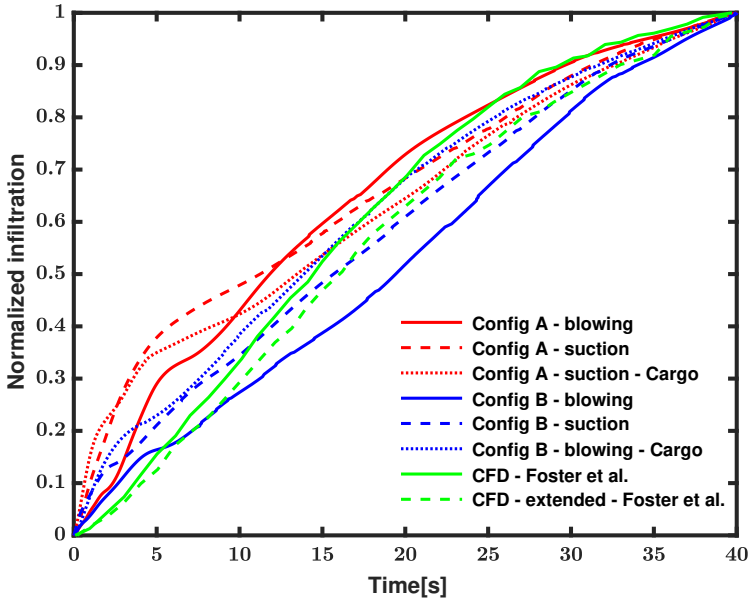

Figure 9: Time evolution of the normalized infiltration compared against the CFD results obtained from Foster et *al.* (Extended; extended boundary CFD model) [13].

Foster et *al.* [13] split the infiltration profile into three regions: lag, steady-state, and tail-off regions. The time evolution of the normalized infiltration, normalized by their given values at $t = 40$ s, exhibits comparable profiles (Fig. 9). Extended boundary CFD model of Foster et *al.* [13] refers to the model with the extended domain from 3 m to 6 m outside the walls of the modelled cold room [13]. For the lag region, from $t = 0$ to $t = 5$ s, the current model demonstrates higher normalized infiltration gradients at the door vertical centerline as the trailer is initialized with the steady-state results with the pre-existing velocity. In the model of Foster et *al.* [13], the fans were turned off 30 s before the door opening. Otherwise, the current model similarly demonstrates a steady-state region from $t = 5$ to $t = 30$ s with a constant normalized infiltration gradient as the infiltration flow is fully developed. The tail-off region from $t = 30$ to $t = 40$ s demonstrates a decreasing normalized infiltration gradient due to the reduced temperature difference between the air inside the trailer and the outside.

Figure 10 shows the temperature at 5 instants and the velocity at $t = 10$ s. At $t = 2.5$ s, the pre-existing flow inside the trailer dominates the flow. Depending on the direction of the rotation of the pre-existing flow inside the trailer, some atmospheric air is dragged into the trailer through the top or bottom regions of the trailer. As infiltration occurs at a relatively high velocity (Fig. 8), peak infiltration occurs within this time interval. However, further infiltration and the penetration of the atmospheric air is limited by the exiting flow acting similar to an air curtain investigated by Foster el *al.* [25], Hayes and Stoecker [26], or Tso et *al.* [14].

Configuration	Renewal time [s]	Peak infiltration rate [$m^3\,s^{-1}$]	Peak infiltration time [s]
A - blowing	14.5	6.7	3.3
A - suction	13.0	10.5	0.7
B - blowing	27.7	3.1	0.3
B - suction	24.5	7.9	0.2

Table 3: Infiltration data from the transient simulations without cargo.

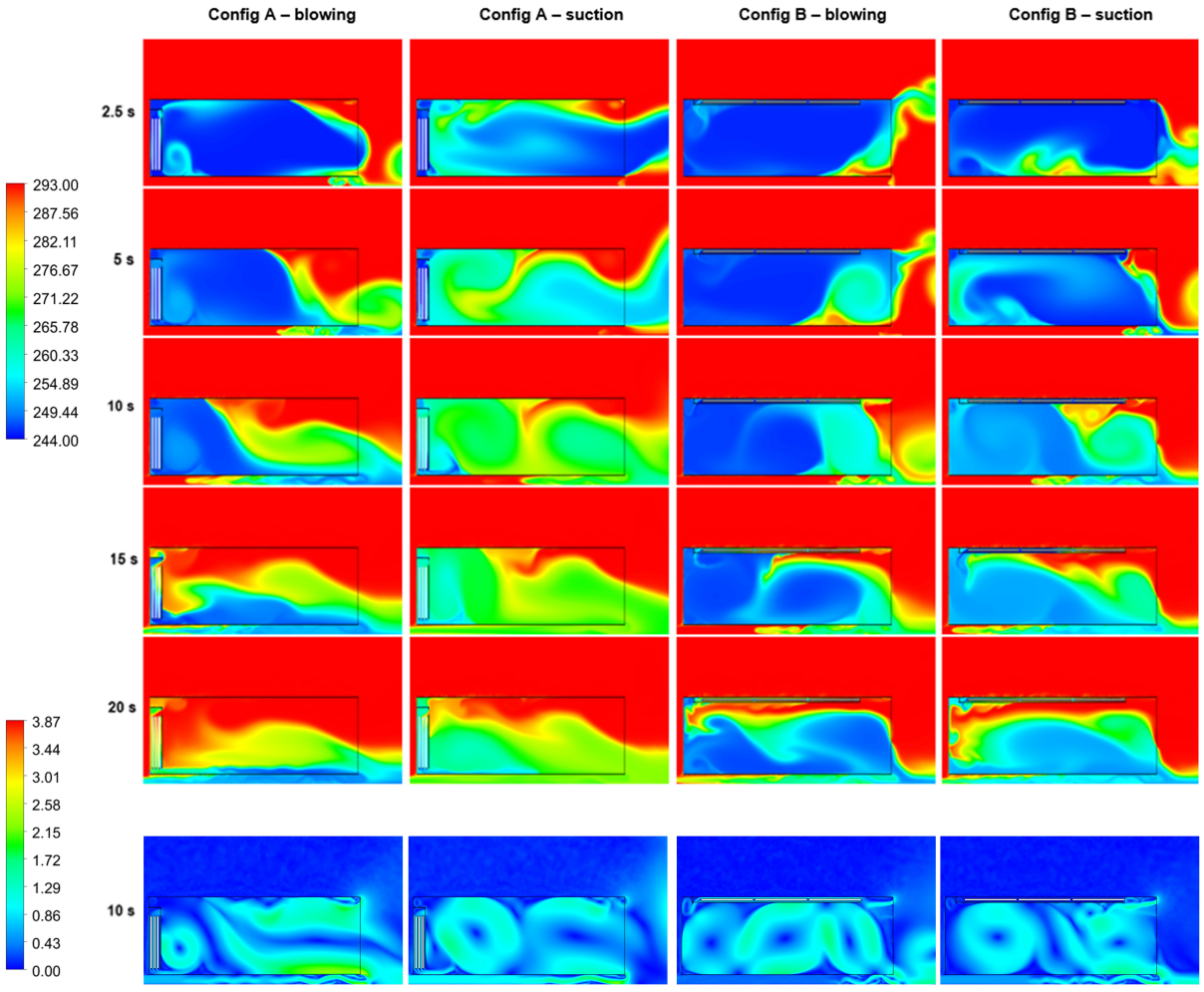

Figure 10: (top) Time evolution of the temperature contours [K] for both configurations and fan modes at five instants; (bottom) Corresponding velocity magnitude contours [ms^{-1}] at $t = 10$ s.

At $t = 5$ s, atmospheric air begins to penetrate through the top region of the doorway into the trailer. The flow regime inside the trailer is still largely dominated by the pre-existing flow and its interaction with

the incoming atmospheric air. Mixing of hot and cold air is still very prominent near the doorway due to this interaction. For Configuration B with blowing mode, infiltration of the atmospheric air through the top region of the doorway cannot be observed until $t = 10$ s due to the exfiltration of the cold high-velocity air through the top of the doorway. From $t = 10$ s, further advancement of the hot atmospheric air into the trailer can be observed. However, due to the presence of the recirculation zones created by the pre-existing flow and the atmospheric air dragged into the trailer before $t = 2.5$ s, further advancement of the atmospheric air into the trailer is limited. This effect can be observed until $t = 15$ s and visualized by the velocity contours in Figure 10b.

At $t = 20$ s, infiltration of the atmospheric air has reached the back of the trailer as the recirculation zones have diminished. During this time, the flow is mostly driven by buoyancy as the influence of the pre-existing flow progressively diminishes over time. The time evolution of the infiltration rate from Figure 8 supports this statement as it is relatively constant until $t = 35$ s. This infiltration dynamics was also observed by Lafaye de Micheaux et *al*. [1] and named "buoyancy driven flow". Moreover, at $t = 35$ s, the infiltration rate decreases slightly as the trailer is now completely filled with the atmospheric air and the infiltration is caused solely by the temperature difference in the plate region. This was also observed by Lafaye de Micheaux et *al*. [1] and named as "boundary layer flow."

Table 3 and Figure 10 show that for either configuration, the operating mode has a minor effect on the renewal time. The blowing mode only takes 11.5% and 13.1% more time to reach the renewal time compared to the suction mode for Configurations A and B, respectively.

However, significant differences are observed between Configurations A and B both from the temperature contours and the time evolution of the infiltration rate. Table 10 shows that Configuration B takes 91.0% and 88.5% longer to reach the renewal time compared to Configuration A with the blowing and suction modes, respectively. The main cause of these differences can be seen from the temperature contours in Figure 10 from $t = 0$ s to $t = 15$ s. For both operating modes, for Configuration B, infiltration of the atmospheric air is mainly due to the high velocity of the cold air near the door, where an air curtain behavior is observed. This limits infiltration and significantly increases the renewal times for Configuration B.

4.2. Influence of the cargo

Similar simulations are performed for the closed and open situations with the presence of cargo.

4.2.1. Closed configurations with cargo

To identify the influence of the cargo loads on the flow development and infiltration, 5 boxes full of frozen meats are placed in the trailer. The first cargo box is located 0.2 m away from the separating wall and 0.15 m above the floor of the trailer to allow for the flow to pass through between the cargo and the floor of the trailer. Proceeding boxes are horizontally separated by 0.1 m. The thermophysical properties of the cargo consisting of frozen meat and cardboard packaging are extracted from Paquette et *al*. [27] and displayed in Table 4. Each box is 1 m long and 1.2 m high. Conduction through the boxes is accounted for in the

simulations and the initial temperature of the cargo is set to 258 K, as the maximum temperature of the frozen foodstuffs is regulated to be below 260.15 K [3].

Material	**Density**	**Specific heat**	**Thermal conductivity**
	$[\mathrm{kg\,m^{-3}}]$	$[\mathrm{J\,kg^{-1}\,K^{-1}}]$	$[\mathrm{W\,m^{-1}\,K^{-1}}]$
Frozen meat	1050	3000	0.25
Cardboard packaging	276	1700	0.058

Table 4: Thermophysical properties of the cargo.

For the transient simulations with cargo, Configuration B - blowing mode was chosen for its better performance in terms of the renewal time. Configuration A - suction mode was also selected as a comparison to keep the direction of the pre-existing flow consistent.

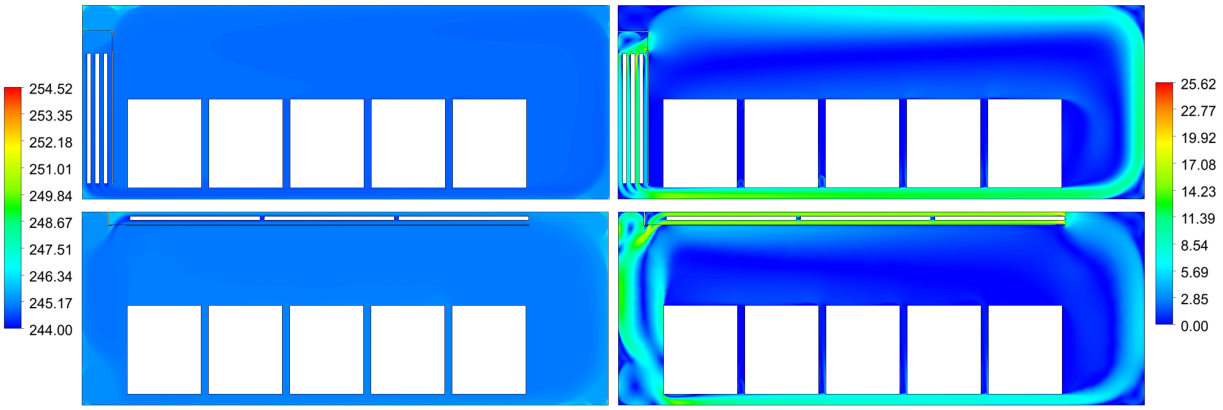

(a) (b)

Figure 11: (a) Temperature [K] and (b) velocity magnitude $[\mathrm{ms^{-1}}]$ contours of Configuration A with cargo (top) and Configuration B with cargo (bottom).

Similar to Section 4.1.1, the temperature distribution inside the trailer remains relatively homogeneous throughout the entire trailer (Fig. 11a). However, the main difference is that for Configuration B, due to the presence of the cargo, the main flow is blocked by the narrow passage between the cargo and the bottom of the trailer. Due to this blockage, a deflection of the flow and a strengthened recirculation zone at the back of the trailer can be observed on Figure 11b. Also, the area-averaged velocity for Configuration B is 31.7 % lower than Configuration A. Consequently, the area-averaged temperature inside the trailer for Configuration B is higher than Configuration A by 0.2 K. On the contrary, for Configuration A, the flow from the fan is directly guided into the passage between the floor of the trailer and the cargo boxes, resulting in neither flow blockage nor strengthened recirculation zones. The homogeneity of the temperature distributions and the maximum temperatures observed inside the trailer similarly meets the regulation criteria discussed in Section 4.1.1.

As shown in Table 5, temperature inside the cargo is nearly homogeneous with a difference of less than 0.1 K. Similarly, the maximum temperature observed inside the cargo for Configuration A is 0.3 K lower than Configuration B.

Configuration	**Area-averaged temperature** [K]	**Area averaged velocity** [$\mathrm{m\,s^{-1}}$]	**Maximum cargo temperature** [K]	**Minimum cargo temperature** [K]
A - suction	244.9	3.24	244.9	244.8
B - blowing	245.1	2.46	245.2	245.1

Table 5: Temperature and velocity magnitude data from the steady-state simulations with cargo.

4.2.2. Door opening period with cargo

The doors are opened at $t = 0$ s for the delivery of the frozen meat and Configurations A and B are compared in terms of infiltration rate.

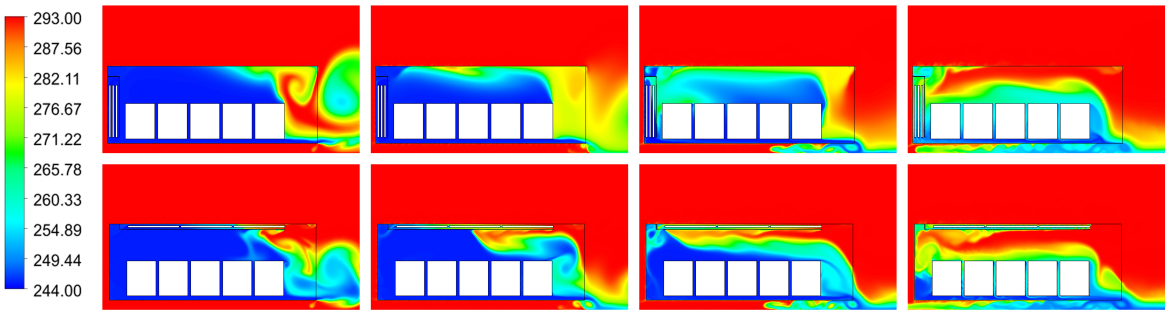

Figure 12: Temperature contours [K] for Configurations A - suction (top) and B - blowing (bottom) at $t = 2.5$, 5, 10 and 20 s (from left to right).

Configuration	**Renewal time** [s]	**Peak infiltration rate** [$\mathrm{m^3\,s^{-1}}$]	**Peak infiltration time** [s]
A - suction - no cargo	13.0	10.5	0.7
A- suction - cargo	25.5	10.7	0.6
B - blowing -no cargo	27.7	3.1	0.3
B - blowing - cargo	25.4	5.3	0.7

Table 6: Infiltration data for Configurations A and B with and without cargo.

The presence of the cargo results in an increase of the renewal time for Configuration A by 96.2% (Table 6)

compared to Configuration A without cargo. However, for Configuration B with cargo, the renewal time decreases by 8.3% with an increase of 71.0% in the peak infiltration rate. As shown in Figure 8, the time evolutions of the infiltration rate and the heat load induced through the door exhibit similar profiles for Configurations A and B with cargo. Peak infiltration occurs at $t = 0.6 \sim 0.7$ s with a near constant infiltration rate from $t \sim 7.5$ s.

Due to the presence of the cargo, recirculation zones seen without the cargo in Figure 10b are no longer observed. As shown in Figure 12, During the first few seconds after the door opening, the cold high-velocity air near the doorway exits the trailer. Then the infiltration of the atmospheric air occurs along the top region of the trailer with the exfiltration of the cold air above the cargo. The area of the infiltration progressively increases before the trailer is completely filled with the atmospheric air. For Configuration A, the renewal time increases due to the infiltration of the atmospheric air being limited by the exiting cold air on top of the cargo. However, for Configuration B, the renewal time decreases as the cargo prevents the formation of the recirculation zones. From the temperature contours on Figure 12, the cargo limits the variation of flow structures that can form inside the trailer and therefore both configurations demonstrate similar flow pattern throughout the simulation. Due to minor temperature changes within the cargo compared to the air inside the trailer, temperature contours of the cargo are excluded from Figure 12.

However, there are minor differences that can be observed between Configurations A and B with cargo. At $t = 2.5$ s, the exiting cold high-velocity air causes stronger mixing to occur for Configuration A. This mixing limits the infiltration of pure atmospheric air into the trailer until $t \sim 10$ s. This is due to the velocity of the pre-existing flow being higher than that of Configuration B as discussed in Section 4.2.1 (Table 5).

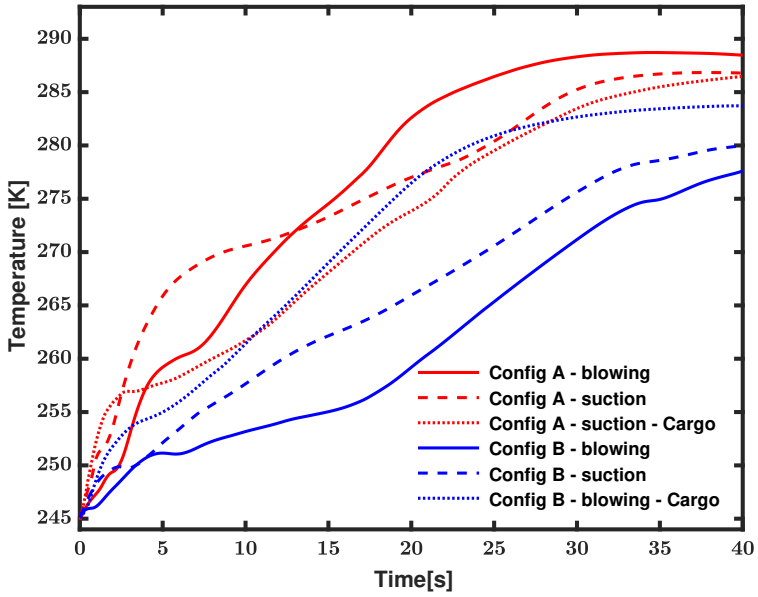

Figure 13: Time evolution of the area averaged temperature inside the trailer.

From Figure 13, the temperature inside the trailer for Configuration B with cargo is higher than Configuration A with cargo for the time interval $t \sim 15$ s to $t \sim 25$ s. As the exiting cold high-velocity air mixing with the atmospheric air limits the infiltration of pure atmospheric air for Configuration A. Regardless, the temperature change of the air inside the trailer for all configurations and operating modes exhibits similar profile to the temperature change observed by Rai et *al.* [17].

Configuration	**Cargo 1**	**Cargo 2**	**Cargo 3**	**Cargo 4**	**Cargo 5**
A - suction	246.7	247.3	247.4	247.6	247.9
B - blowing	247.5	249.1	249.9	249.8	249.8

Table 7: Maximum temperature [K] of the cargo at $t = 40$ s.

As the temperature change is higher for Configuration B after the cold high-velocity air exits the trailer, from Table 7, the maximum temperature observed at each cargo box after 40 seconds is significantly higher for Configuration B (locations of each cargo box described in Section 4.2.1). The temperature difference between the cargo boxes is greater than the initial maximum temperature difference of 0.3 K (Table 5). A maximum temperature difference of 2.5 K for Cargo 3 and a minimum temperature difference of 0.8 K is observed for the inner-most cargo (Cargo 1) between Configurations A and B, respectively. For Configuration B, the highest cargo temperature is observed by Cargo 3 as the exiting cold air on top of the cargo and the recirculation zones at the back of the trailer mixing with the infiltrated atmospheric air limits other cargo boxes from making contact with the hot air. For Configuration A, the highest cargo temperature is observed by the outer-most cargo (Cargo 5), as the exiting cold air mixed with the atmospheric air makes the earliest contact and increases its temperature. The maximum cargo temperatures observed are still below the regulated temperature for quick (deep) frozen foodstuffs at 255.15 K [3].

5. Conclusions

A numerical model has been developed and validated to predict the turbulent flow and heat transfer inside a refrigerated truck trailer equipped with eutectic plates. The model has been validated against the experimental data of Lafaye de Micheaux et *al.* [1]. It was shown that the 3D effects did not influence significantly the velocity and temperature distributions at the midplane of the doorway. The $k-\omega$ SST model slightly improved the predictions of the realizable $k-\epsilon$ model of Lafaye de Micheaux et *al.* [1]. Based on the developed model, a 2D model was adapted to optimize the configuration of the refrigeration system with the eutectic plates in terms of trailer and cargo temperatures by analyzing the air flow and the infiltration heat load into the refrigerated truck trailer during the door opening period. Without cargo, the configuration with the plates placed in series on the roof of the trailer noticeably improved the performance in terms of trailer temperature with respect to the configuration with the plates in series placed at the back. However, the presence of a cargo eliminates the recirculation zones that prevented the infiltration of the atmospheric air. Also, for the configuration with the plates placed on the roof, a lower initial velocity of the pre-existing

flow inside the trailer was observed caused by the blockage of the flow due to the cargo. Therefore, the atmospheric air was able to infiltrate and increase the temperature of the trailer quicker and resulted in a higher maximum temperature observed for the cargo.

As the number of cargo boxes will progressively decrease during the delivery cycle, it is plausible that the configuration with the plates placed on the roof could improve the performance as the influence of the pre-existing flow seen without the cargo will progressively emerge. The influence of the cargo parameters such as cargo locations, dimensions, arrangements, etc, should be investigated into more details as it has a significant influence over the development of the pre-existing flow inside the trailer. Further development should include a multiphase model to account for both the humidity of air and the melting of the phase change material inside the plates. Another major concern is that the formation of frost along the plates could interfere with the heat transfer between the plates and the surrounding air.

Acknowledgments

This project is part of the NSERC Chair on Industrial Energy Efficiency, established at Université de Sherbrooke in 2019, with the support of Hydro-Québec, Natural Resources Canada and Emerson Commercial & Residential Solutions. All the computations have been performed using the facilities provided by Calcul Québec. They are all here gratefully acknowledged.

References

[1] T. Lafaye de Micheaux, M. Ducoulombier, J. Moureh, V. Sartre, J. Bonjour, Experimental and numerical investigation of the infiltration heat load during the opening of a refrigerated truck body, International Journal of Refrigeration 54 (2015) 170–189.

[2] S. Tassou, G. De-Lille, Y. Ge, Food transport refrigeration–approaches to reduce energy consumption and environmental impacts of road transport, Applied Thermal Engineering 29 (8-9) (2009) 1467–1477.

[3] UN Economic Commission for Europe – Inland Transport Committee, ATP as amended on 6 January 2018 – Agreement on the International Carriage of Perishable Foodstuff and on the Special Equipment to be used for such Carriage, Tech. rep. (2018).

[4] S. Croquer, A. E. Benchikh Le Hocine, S. Poncet, Numerical modelling of heat and mass transfer in a refrigerated truck trailer, in: V. Minea (Ed.), Proceedings of the 25th IIR International Congress of Refrigeration, International Institute of Refrigeration, Montreal, Canada, 2019, pp. 3574–3581.

[5] M. Bonaventure, A. E. Benchikh Le Hocine, S. Croquer, K. Huchtemann, S. Poncet, Heat and mass transfer in a loaded truck trailer equipped with eutectic plates: a comparative numerical study, in: Proceedings of the 6th IIR Conference on Sustainability and the Cold Chain ICCC2020, International Institute of Refrigeration, Nantes, France, 2020, pp. 494–499.

[6] S. Tassou, J. Lewis, Y. Ge, A. Hadawey, I. Chaer, A review of emerging technologies for food refrigeration applications, Applied Thermal Engineering 30 (4) (2010) 263–276.

[7] A. Tinti, A. Tarzia, A. Passaro, R. Angiuli, Thermographic analysis of polyurethane foams integrated with phase change materials designed for dynamic thermal insulation in refrigerated transport, Applied Thermal Engineering 70 (1) (2014) 201–210.

[8] B. Copertaro, P. Principi, R. Fioretti, Thermal performance analysis of PCM in refrigerated container envelopes in the Italian context - Numerical modeling and validation, Applied Thermal Engineering 102 (2016) 873–881.

[9] B. Michel, P. Glouannec, A. Fuentes, P. Chauvelon, Experimental and numerical study of insulation walls containing a composite layer of PU-PCM and dedicated to refrigerated vehicle, Applied Thermal Engineering 116 (2017) 382–391.

[10] A. Azzouz, J. Gossé, M. Duminil, Détermination expérimentale des pertes de froid occasionnées par l'ouverture d'une porte de chamber froide industrielle, Revue Internationale du Froid 16 (1) (1993) 57—66.

[11] P. Chen, D. Cleland, S. Lovatt, M. Bassett, An empirical model for predicting air infiltration into refrigerated stores through doors, International Journal of Refrigeration 25 (6) (2002) 799–812.

[12] M. Hoang, P. Verboven, J. D. Baerdemaeker, B. Nicolai, Analysis of the air flow in a cold store by means of computational fluid dynamics, International Journal of Refrigeration 23 (2000) 127–140.

[13] A. Foster, M. Swain, R. Barrett, S. James, Experimental verification of analytical and CFD predictions of infiltration through cold store entrances, International Journal of Refrigeration 26 (8) (2003) 918–925.

[14] C. Tso, S. Yu, H. Poh, P. Jolly, Experimental study on the heat and mass transfer characteristics in a refrigerated truck, International Journal of Refrigeration 25 (3) (2002) 340–350.

[15] F. Clavier, V. Sartre, J. Bonjour, Infiltration heat load through the doorway of a refrigerated truck protected with an air curtain, Proceedings of the 23th International Congress of Refrigeration, International Institute of Refrigeration, Prague, 2011.

[16] M. Lejeune, Optimisation du couplage entre froid statique et inertie thermique - application à un véhicule de livraison à domicile de produits surgelés, Ph.D. thesis, Université Pierre et Marie Curie (2016).

[17] A. Rai, J. Sun, S. Tassou, Numerical investigation of the protective mechanisms of air curtain in a refrigerated truck during door openings, Energy Procedia 161 (2019) 216–223.

[18] A. Rai, J. Sun, S. Tassou, Three-dimensional investigation on the positioning of air curtain on its effectiveness in refrigerated vehicles used for food distribution, Energy Procedia 161 (2019) 224–231.

[19] M. B. Taher, M. Mahdaoui, T. Kousksou, Y. Zeraouli, M. Ahachad, Numerical study of the aero-thermal performance for different scenarios of a refrigerated truck using urans, Journal of Cleaner Production 320 (2021) 128775.

[20] P. B. T. Jara, J. J. A. Rivera, C. E. B. Merino, E. V. Silva, G. A. Farfán, Thermal behavior of a refrigerated vehicle: Process simulation, International Journal of Refrigeration 100 (2019) 124–130.

[21] A. Mousazade, R. Rafee, M. S. Valipour, Thermal performance of cold panels with phase change materials in a refrigerated truck, International Journal of Refrigeration 120 (2020) 119–126.

[22] D. Gray, A. Giorgini, The validity of the Boussinesq approximation for liquids and gases, International Journal of Heat and Mass Transfer 19 (5) (1976) 545–551.

[23] F. R. Menter, Two-equation eddy-viscosity turbulence models for engineering applications, AIAA Journal 32 (8) (1994) 1598–1605.

[24] P. Glouannec, B. Michel, G. Delamarre, Y. Grohens, Experimental and numerical study of heat transfer across insulation wall of a refrigerated integral panel van, Applied Thermal Engineering 73 (1) (2014) 196–204.

[25] A. Foster, M. Swain, R. Barrett, P. D'Agaro, S. James, Effectiveness and optimum jet velocity for a plane jet air curtain used to restrict cold room infiltration, International Journal of Refrigeration 29 (5) (2006) 692–699.

[26] F. Hayes, W. Stoecker, Design data for air curtains, Ashrae Transactions 75 (2) (1969) 168–180.

[27] J. C. Paquette, S. Mercier, B. Marcos, S. Morasse, Modeling the thermal performance of a multilayer box for the transportation of perishable food, Food and Bioproducts Processing 105 (2017) 77–85.

- Heat infiltration was analyzed during the door opening period.
- Influence of eutectic plate locations and fan operating modes were investigated.
- Recirculation zones inside the trailer limited the infiltration.
- Presence of cargo eliminated the recirculation zones inside the trailer.

Declaration of interests

☒ The authors declare that they have no known competing financial interests or personal relationships that could have appeared to influence the work reported in this paper.

☐ The authors declare the following financial interests/personal relationships which may be considered as potential competing interests: